

FINAL REPORT

ANALYTICAL AND EXPERIMENTAL EVALUATION OF AN INNOVATIVE ALUMINUM BRIDGE DECK PANEL

PART I: SERVICE LOAD PERFORMANCE

Jeffrey M. Dobmeier
Graduate Research Assistant

Furman W. Barton, Ph.D., P.E.
Faculty Research Scientist

José P. Gomez, Ph.D., P.E.
Senior Research Scientist

Peter J. Massarelli, Ph.D.
Faculty Research Associate

Wallace T. McKeel, Jr., P.E.
Research Manager

INTRODUCTION

Deck deterioration is responsible for the majority of deficient bridge ratings in the United States (Sotiropoulos & GangaRao, 1993). Subject to dynamic loading, cyclic loading, and occasional overloading, bridge decks are the most severely stressed elements in a bridge (Wolchuk, 1987). Combined with the stresses induced by environmental effects such as temperature variations, moisture variations, and freeze-thaw cycles, it is easy to see why the Federal Highway Administration estimates that 7,000 bridge decks are in need of immediate replacement (The Aluminum Association, 1996).

Deck deterioration is accelerated by corrosion problems. De-icing salts applied to bridge decks eventually penetrate the concrete and corrode the reinforcing steel. The corroding steel, in turn, causes the deck to crack, spall, and delaminate. This damaged concrete is more susceptible to additional permeation of harmful chemicals, thus accelerating the process of deck deterioration. Steel decks, although not as common as concrete, are also prone to corrosion.

Many potential solutions have evolved in the hopes of limiting corrosion damage. Less permeable concrete, cathodic protection systems, and protective coatings are just a few of the methods being examined. Another approach to eliminating this corrosion problem is the use of alternative materials such as aluminum.

Aluminum holds considerable promise due to its ease of manufacture and its excellent corrosion resistance. Not only can the metal survive harsh environments, it can do so without any protective coatings (Kissell & Ferry, 1995; Sharp, 1993). This capability is a result of pure aluminum's unusual property of oxidizing rapidly when exposed to air, where it produces a hard layer that is highly resistant to corrosion (Sharp, 1993). This automatic oxidation also adds to the benefit of self-repair. If the surface of an aluminum component is damaged, bare aluminum becomes exposed and rapidly oxidizes, preserving the corrosion resistance. Conversely, most non-aluminum materials that are coated for corrosion resistance become vulnerable to chemical degradation if the coating is damaged.

Reynolds Metals Company (Reynolds) believes that aluminum components can provide a long lasting, durable infrastructure. Reynolds has invested considerable resources to develop their proprietary aluminum deck system. Once these decks were developed, Reynolds approached several state departments of transportation in hopes of securing projects to showcase their new system.

Interested in the potential for long-term savings, the Virginia Department of Transportation agreed to employ the deck system in two projects. A single-span bridge located on U.S. Route 58 was chosen for the first project. Using the aluminum deck in a new superstructure, the bridge was widened by 1.83 m (6 ft) to remove it from the functionally obsolete list (*New Aluminum Decks*, 1996). Originally, the second project that was planned was supposed to involve a continuous span bridge on Virginia's Smart Highway, the state test bed for intelligent transportation systems and materials. However, recent complications with fabrication of the second deck have delayed initiation of the second project.

Since this aluminum bridge venture involved new technologies, it was classified as an experimental project and required a thorough evaluation. Using Federal Highway Administration sponsorship, the Virginia Transportation Research Council initiated a three-phase study of the Reynolds deck system.

The first phase of the study focused on evaluating the static response of a 2.74 m x 3.66 m (9 ft x 12 ft) deck panel. Both experimental and analytical response information were used in the evaluation process. Experimental response data was obtained from seven service-load tests and two ultimate-load tests conducted in the fall of 1996 at the Turner-Fairbank Structural Laboratory. Analytical response information was generated from finite element models developed to accurately represent the deck panel. The evaluation of the deck panel for service loads and the response information from laboratory tests and finite element models are presented in this report. Evaluation of the panels based on ultimate load tests will be described in a subsequent report.

Phase 2 of the study, which has already been completed, focused on a field evaluation of the completed bridge. This involved a series of static and dynamic load tests of the completed bridge and the development and response of a finite element model of the bridge.

The final phase of the study will focus on the long-term behavior of the aluminum deck system. Evaluation of this behavior will be concerned with durability of the wearing surface and on fatigue behavior of the deck system. Fatigue tests will be conducted on a modified deck panel at the Virginia Polytechnic Institute and State University, and nondestructive test methods will then be used to assess the condition of the fatigued panels prior to ultimate-load tests.

PURPOSE AND SCOPE

The purpose of this study was to evaluate the service-load behavior of an aluminum deck panel by developing finite element models that could predict panel responses and by conducting static load tests in the laboratory and measuring the responses of these load tests.

METHODOLOGY

The specific objective of this study was to develop accurate finite element models of the deck panel that would enable researchers to obtain a more complete understanding of the structural response. Models were created to simulate the seven service-load tests. Accuracy was verified by comparing analytical strains and displacements to the corresponding experimental values. Once accuracy was confirmed, the models were employed to analyze response mechanisms. This report documents the findings from the service load simulations.

The methodology developed in this study, although concerned with only one aluminum deck panel, has much broader applications. The procedure can be effectively used for evaluating the response and for the design validation of any new deck system.

Deck System

The deck system analyzed in this study consisted of an assemblage of the two-voided extrusion shown in Figure 1. These extrusions were fabricated from 6063-T6 aluminum, which has a minimum tensile yield strength of 172.4 MPa (25 ksi) and a minimum ultimate strength of 206.8 MPa (30 ksi). The deck was fabricated by welding extrusions together at the top and bottom flanges to achieve the desired dimensions.

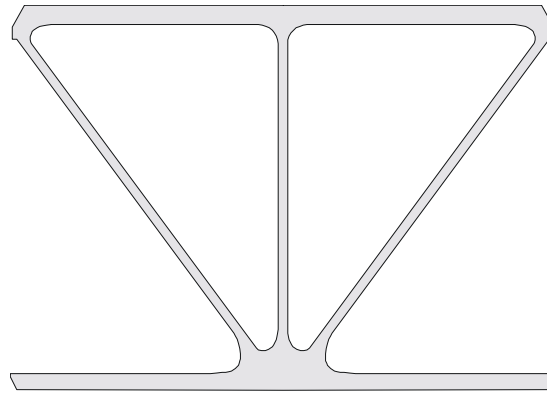
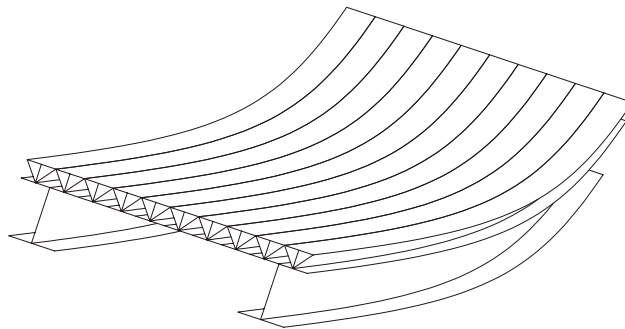
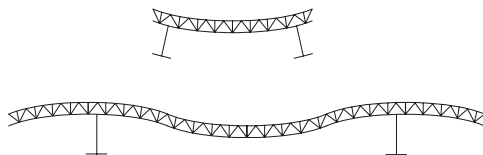


Figure 1. Extrusion Cross Section

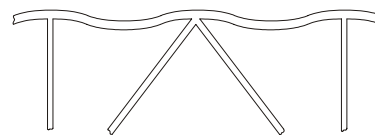
Although the resulting deck was nearly isotropic, the panel was typically oriented with extrusions parallel with the supporting girders and the flow of traffic. When installed in this manner, the stresses developed under loading can be categorized into the three stress systems, indicated schematically in Figure 2. System I stresses were generated by longitudinal bending of the composite panel-girder unit. System II stresses resulted from the panel bending transversely between the supporting girders. System III stresses were the local effects present in the vicinity of the concentrated wheel loads and resulted from transverse bending of the top flange between the stiffeners.



System I Stresses—Longitudinal Bending of the Composite Deck/Girder Section



System II Stresses—Transverse Bending of the Deck Between Girders



System III Stresses—Localized, Transverse Bending of the Top Deck Flange

Figure 2. Three Stress Systems Developed in the Deck

Experimental Evaluation

The laboratory tests for this project were conducted at the Turner-Fairbank Highway Research Center in Langley, Virginia. A small deck panel measuring 2.74 m x 3.66 m (9 ft x 12 ft) served as the test specimen. This panel was composed of nine extrusions, each measuring 0.30 m (1 ft) wide and 3.66 m (12 ft) long. An illustration of the system is provided in Figure 3. Sixteen strain rosette gages were installed at strategic locations on the bottom surface of the panel. A strain rosette consisted of three separate gages with the gages orientated at 0, 45 and 90 degrees. In these tests, the rosettes were oriented such that the orthogonal elements of the gage were parallel with the panel centerlines. To record the data, each gage of each rosette was assigned a channel number in the data acquisition system. Thus, channel numbers 1 through 3 were assigned to rosette 1, channel numbers 4 through 6 to rosette 2, etc. Figure 4 shows the numbering and location of the rosettes, with dimensions representing the distance to the origin of the rosettes.

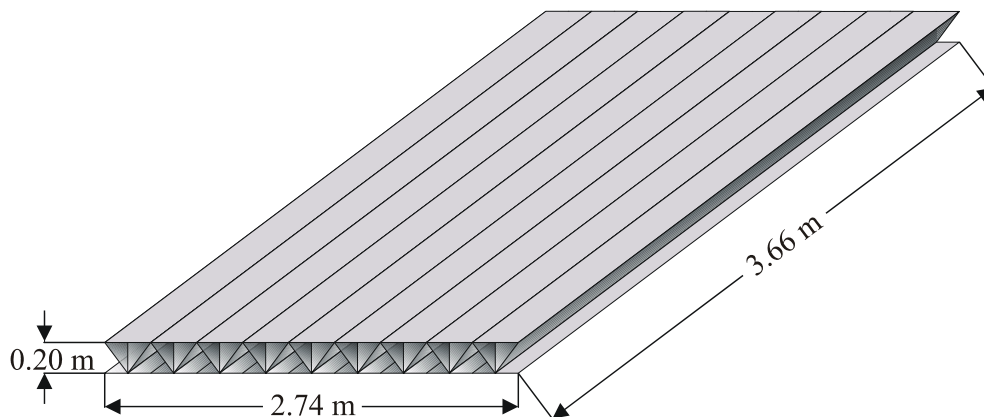


Figure 3. Dimensions of the Panel Tested in the Laboratory

Twenty-eight rosette gages were installed on the top surface of the panel. Additional gages were used on the upper surface due to the presence of the load patch, which was expected to introduce localized (System III stresses) phenomena. It was hoped that the installation of extra gages would capture this type of response. Rosettes were numbered consecutively, continuing where the bottom panel gage numbering stopped. The same mapping scheme was used to assign channel numbers to the elements of the rosettes. Figure 5 illustrates the layout of the gages on the top deck surface.

In addition to recording strain data, displacement and rotation data were also obtained. Seven deflection gages were connected to the bottom of the panel to record displacement data. The locations of these gages varied with each test. Four tiltmeters were also mounted on the top deck surface. Combined with the strain rosettes, this instrumentation plan required 144 discrete channels to record the data.

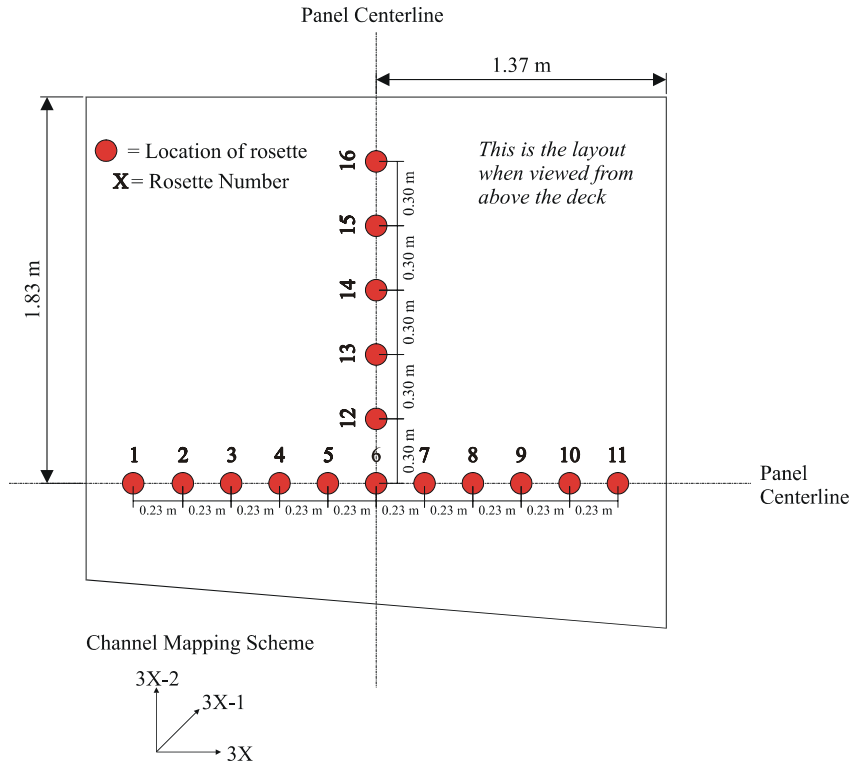


Figure 4. Location of Rosettes on the Bottom Deck Surface

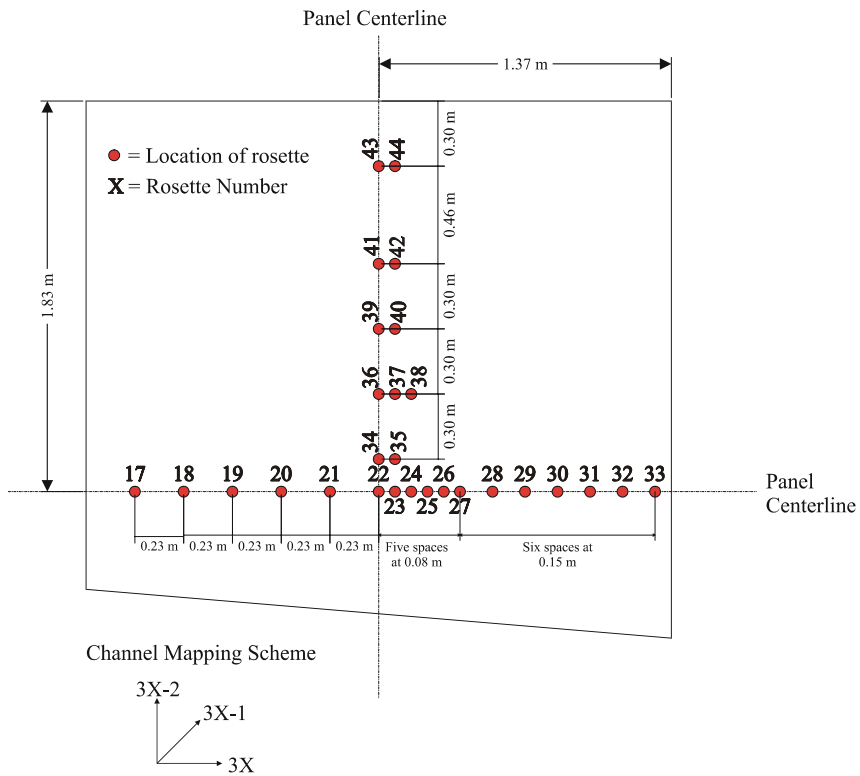


Figure 5. Location of Rosettes on the Top Deck Surface

All seven service-load tests used the same load magnitude; however, they used different boundary conditions and load placement. These different boundary conditions and loading configurations were intended to replicate the scenarios typically encountered during actual service conditions. Figures 6 and 7 illustrate the different configurations used in each test. The magnitude and patch size of the service load was based upon the 1994 AASHTO LRFD Bridge Design Specifications. According to these specifications, the dual wheels of an HS-20 truck generate a 94.75 kN (21,300 lb) force. The tires distribute this force over a 50.80 cm x 21.59 cm (20 in x 8.5 in) load patch. Laboratory tests used a neoprene patch to simulate the contact area, whereas load cells recorded the actual load applied during the various tests. Figure 8 shows the actual panel and experimental setup.

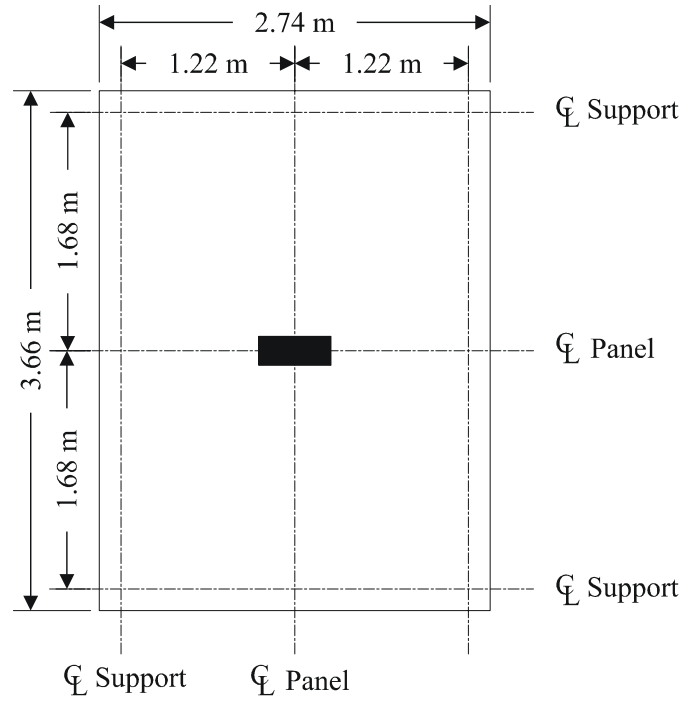
The service loads were applied at the rate of 222.41 N per second (50 lb per second). Gage readings were taken approximately every 4.45 kN (1,000 lb). Loading was stopped once the magnitude reached the 94.75 kN (21,300 lb) mark, and data were recorded. The panel was then unloaded at the same rate, and data were recorded with the same frequency. Once unloaded, the gages were scanned to see if any residual strains were present.

Few difficulties were encountered during the experimental study. The problems encountered were minor. One of the seven deflection gages did not work; therefore, the amount of displacement data recorded was less than anticipated. The clamping mechanism used to simulate the fixed-end boundary conditions in the laboratory did not provide complete fixity and, as a result, the raw deflection and rotation data recorded during these two tests were not accurate. Fortunately, gages installed at the fixed end measured the slippage, which allowed the ill-conditioned data to be corrected during post-processing.

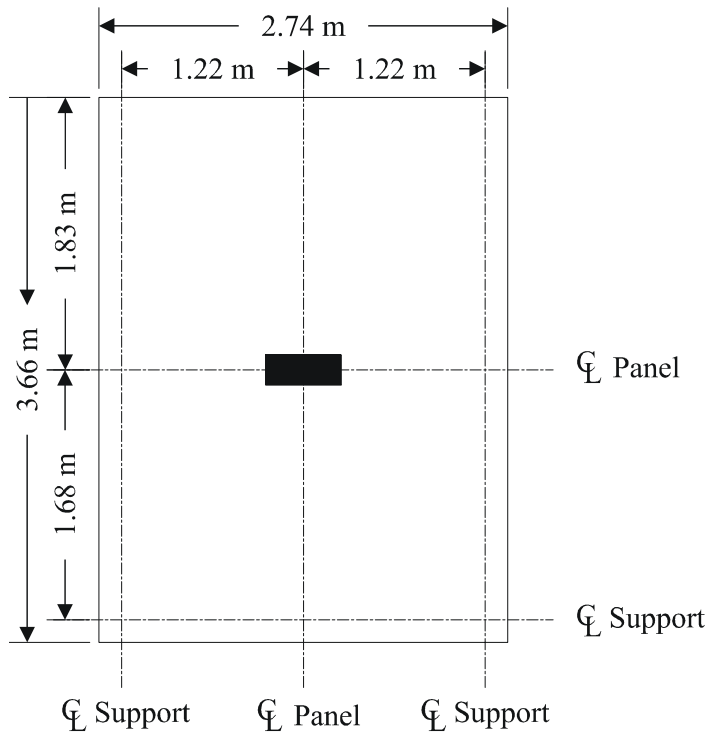
Analytical Evaluation

Models for the seven service-load tests were developed on the large-scale, general-purpose finite element code ABAQUS. Models for load cases 1, 2, 3, and 7 were developed first, since the same mesh could be used for each simulation. This allowed researchers to assess the effects of various parameters on model accuracy with minimal work. Once the most accurate models were identified, modifications were made to accommodate load cases 4, 5, and 6. The primary adjustment for these load cases was modification of the mesh to handle the new position of the load patch. Figures 6 and 7 illustrate these load cases.

For all of the simulations, model refinement was driven by the accuracy of output. New models were initially examined visually to identify gross errors or mistakes. Next, the output files were scanned for warnings and error messages. The strain and displacement data were then compared to laboratory observations. Both the magnitude and distribution were compared. Checks on symmetry were also considered when appropriate.

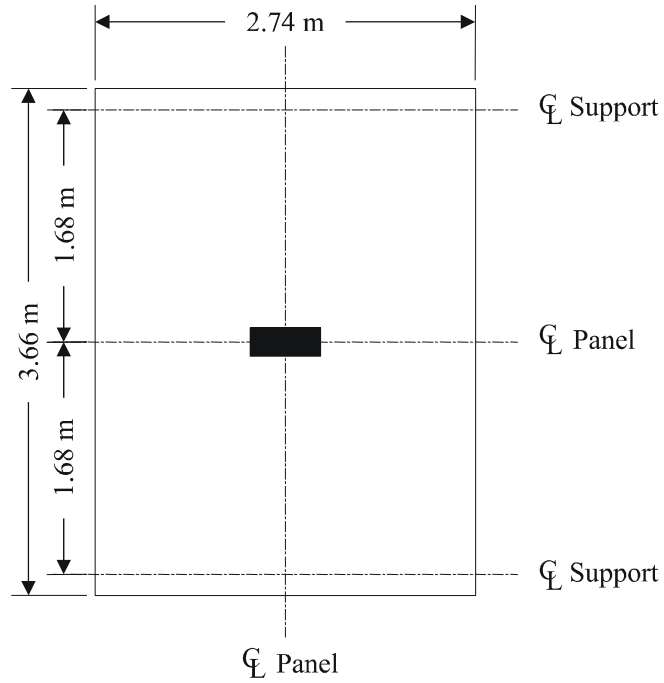


Load Case One

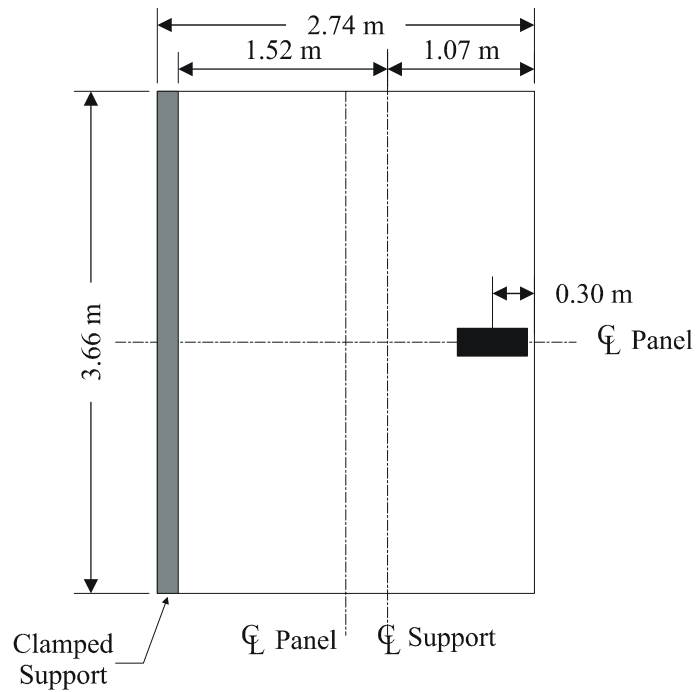


Load Case Two

Figure 6. Load Cases One and Two (Continued)

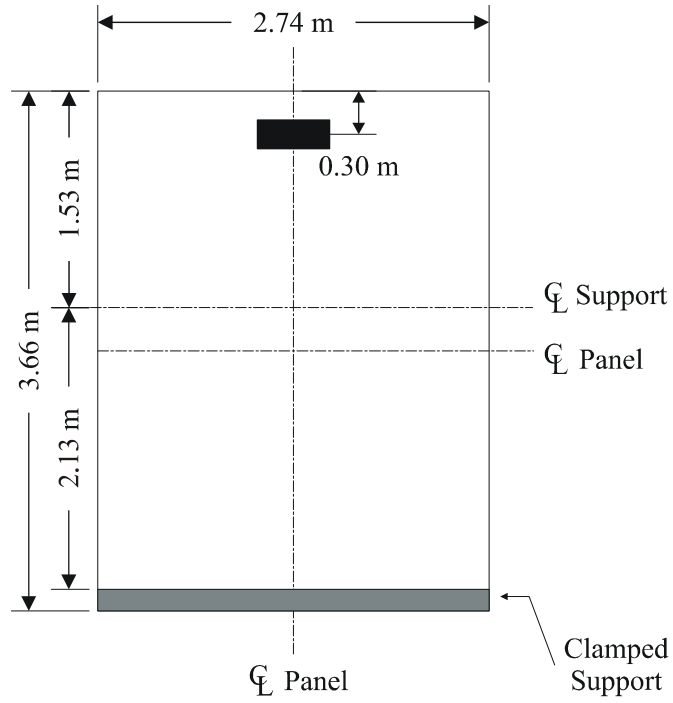


Load Case Three

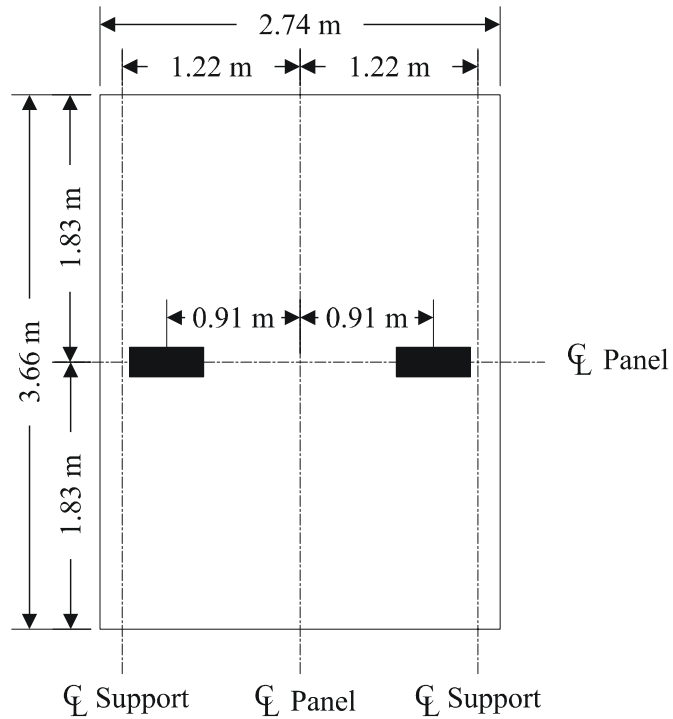


Load Case Four

Figure 6. Load Cases Three and Four (Continued)

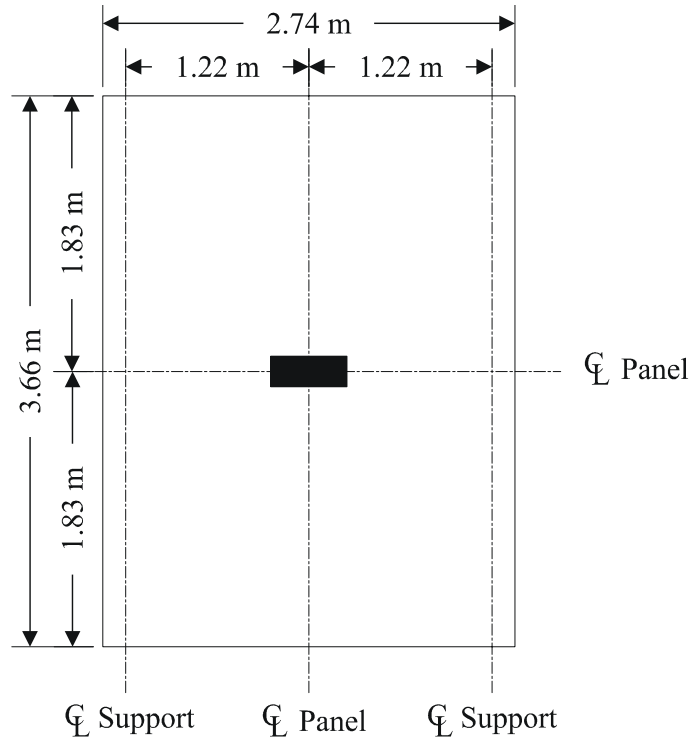


Load Case Five



Load Case Six

Figure 7. Load Cases Five and Six (Continued)



Load Case Seven

Figure 7. Load Case Seven (Continued)



Figure 8. Actual Panel Test at the Federal Highway Administration

The following terminology was used in this study to identify structural members and directions on the panel. The three types of web stiffeners were classified by their orientation. The stiffeners with no incline were called vertical stiffeners, although the inclined stiffeners were identified as simply inclined regardless of their orientation. Figure 9 illustrates this notation. Another identification scheme was used to identify the elements that represented the top and bottom surfaces of the deck. This system helped to identify the top and bottom plates that bound the stiffeners. The top member was referred to as the top deck surface or the top chord, and the bottom member was called the bottom deck surface or the bottom chord. This designation arose from the truss-style design of each extrusion. Figure 10 depicts the various members and their locations.

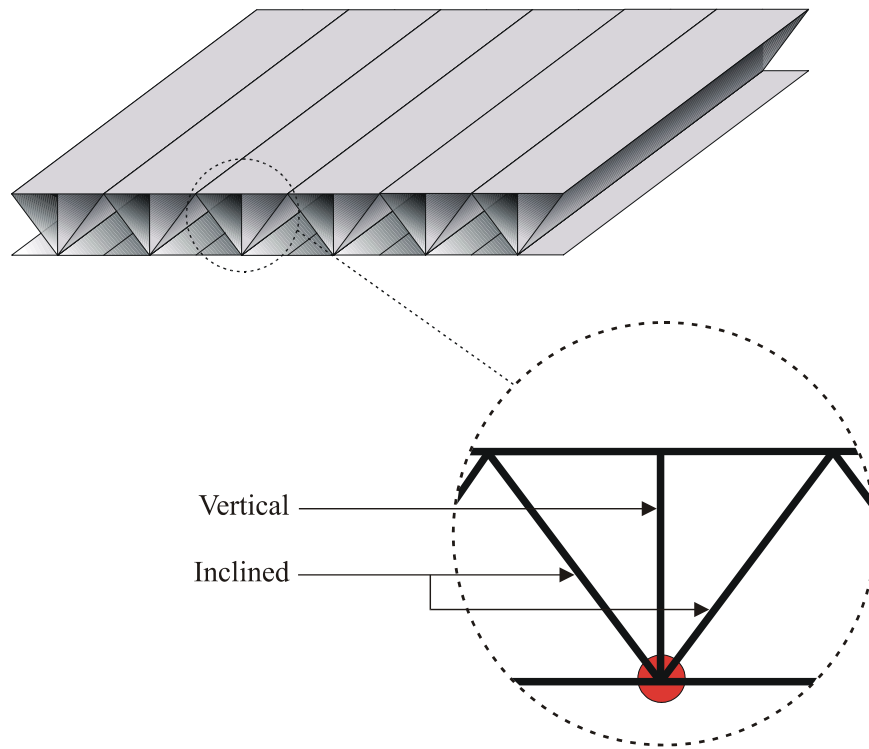


Figure 9. Nomenclature of the Stiffeners

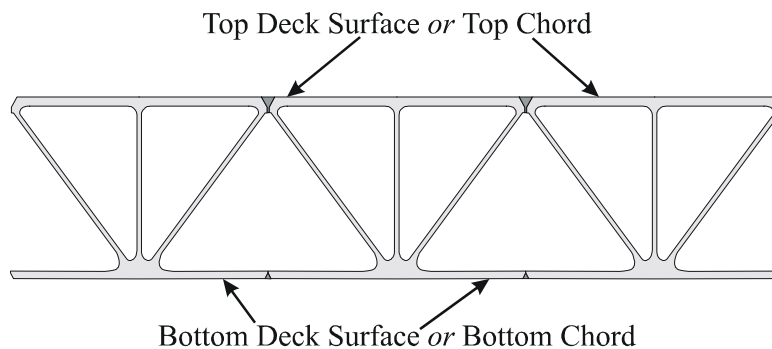


Figure 10. Nomenclature of Top and Bottom Deck Surfaces

Directions were specified with respect to two mutually perpendicular axes where the origin coincides with the geometric center of the panel. Regardless of the support conditions, the direction parallel with the extrusions was called the longitudinal direction and the direction perpendicular to the extrusions was referred to as the transverse direction. This convention system arose from the orientation of the panel in an actual bridge. The illustration in Figure 11 clarifies this directional system.

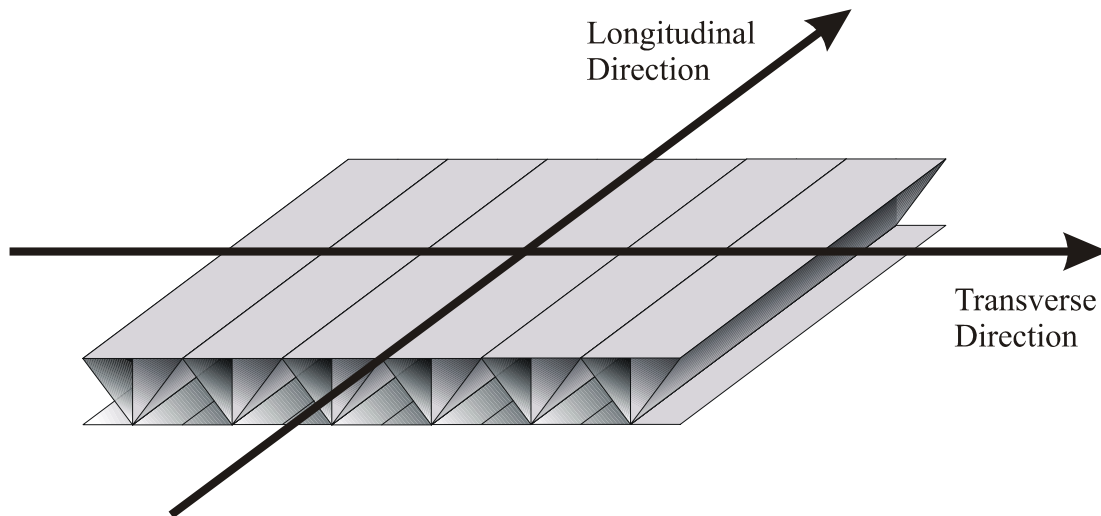


Figure 11. Direction Nomenclature

Mesh Generation

The development of a mesh was the step that actually discretized the continuous system into a finite number of elements. Meshes should be dense enough to capture high gradients, yet simple enough to expedite the solution process. Regular, repeating patterns were desirable as they facilitated automatic generation of both the mesh and the elements. Additional mesh guidelines were established by considering the elements that were expected to be used as well as the expected solution.

Six different meshes were developed and tested on load cases 1, 2, 3, and 7. These meshes used various discretization schemes for the deck surfaces and stiffeners. Results from models based upon these meshes were then compared to experimental values. Based upon this verification process, two specific meshes were chosen for future use. The first mesh discretized the top and bottom deck surfaces into 7.62-cm (3-in) squares. Each stiffener was modeled with two rows of elements per stiffener height. Several triangular regions were also included in this mesh to accommodate the load patch. A picture of this mesh is shown in Figure 12.

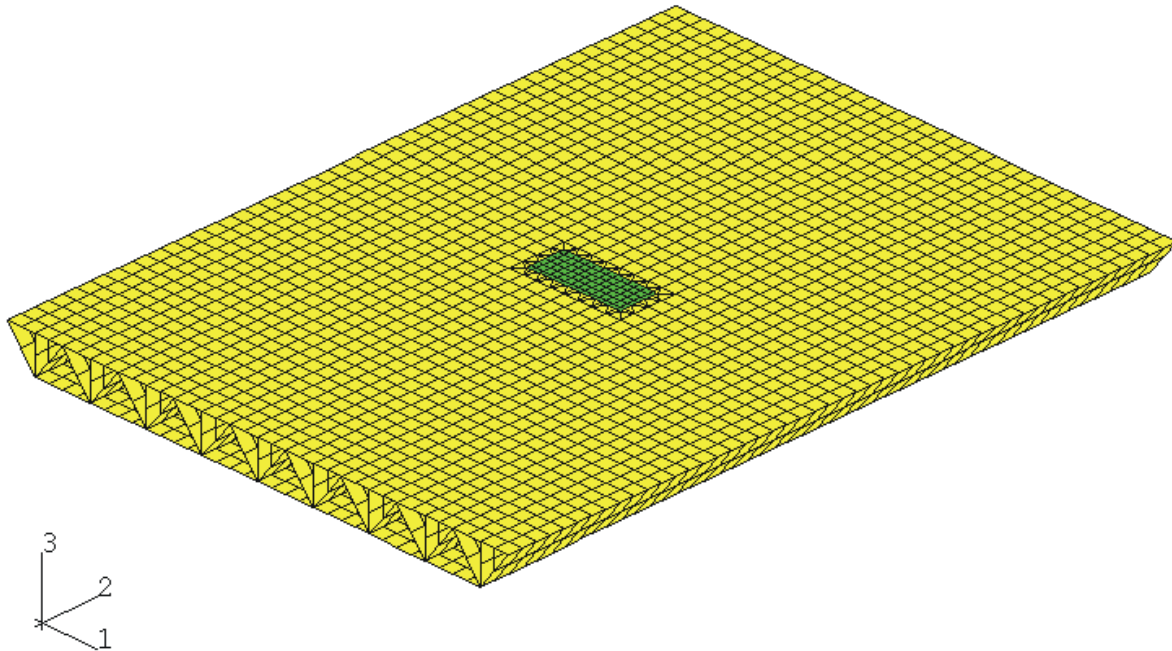


Figure 12. First Mesh For Load Cases One, Two, Three, And Seven (3 X 3 Discretization With Two Rows of Elements Per Stiffener's Height)

The second mesh used a finer discretization for both the deck surfaces and the stiffeners. The top and bottom deck surfaces were divided into 5.08 cm (2 in) squares. Each stiffener was discretized with four rows of elements per stiffener height. Unlike the other mesh, no triangular regions were included in this system. Figure 13 illustrates this mesh.

Meshes were then developed for load cases 4, 5, and 6. The mesh using 7.62 cm (3 in) squares on the deck surfaces required certain modifications to accommodate the load patch. The necessary adjustments varied for each load case. Pictures of the meshes used in simulating load cases 4, 5, and 6 are illustrated in Figures 14, 15, and 16, respectively. The mesh using the 5.08 cm (2 in) squares on the deck surfaces did not require any modification to accommodate the load patch in these load cases and can be viewed in Figure 13.

Although mesh refinement requires substantial time and effort, element selection was equally important. ABAQUS has an extensive library of elements to choose from, each with their own properties. Based upon problem criteria and element characteristics, solid (continuum) elements and shell elements were considered for these models.

The aluminum deck resisted loading primarily through plate-bending mechanisms. First-order solid elements have difficulty replicating pure bending response (Cook, Malkus, & Plesha, 1989). Although higher-order elements generally avoid such problems, they are computationally more expensive. Solid elements also need to be well shaped and possess suitable aspect ratios to promote accurate results. Furthermore, thinned-down solid elements still exhibit transverse strain, which may lead to numerical difficulties.

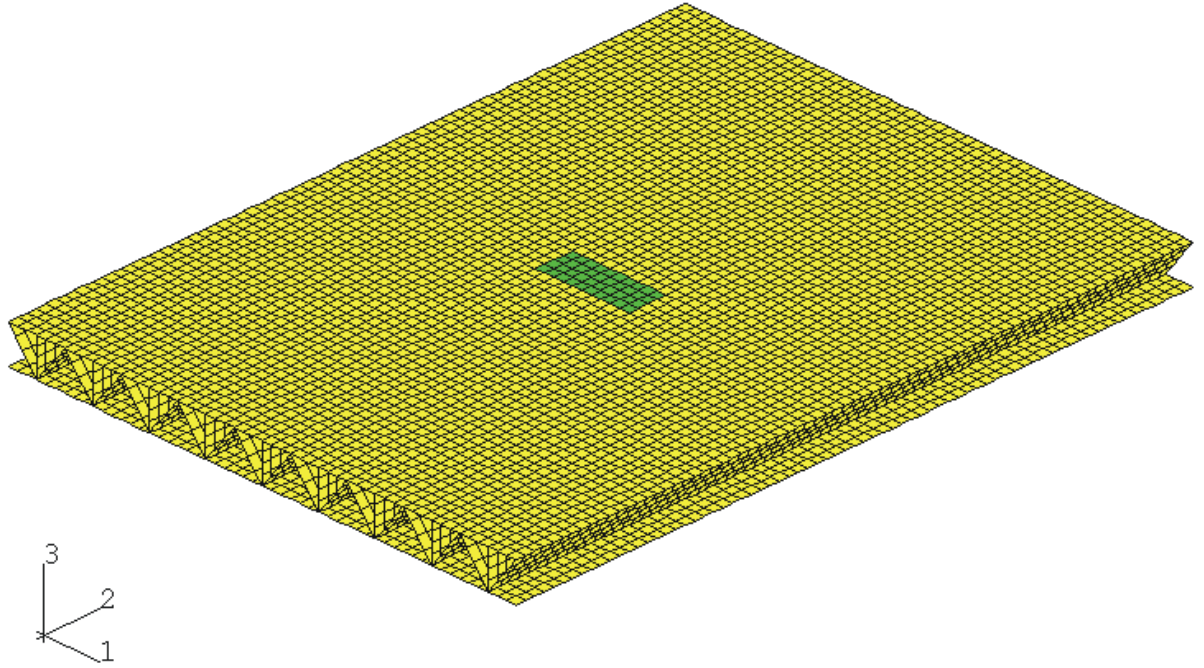


Figure 13. Second Mesh For Load Cases One, Two, Three And Seven (2 X 2 Discretization With Four Rows of Elements Per Stiffener Height)

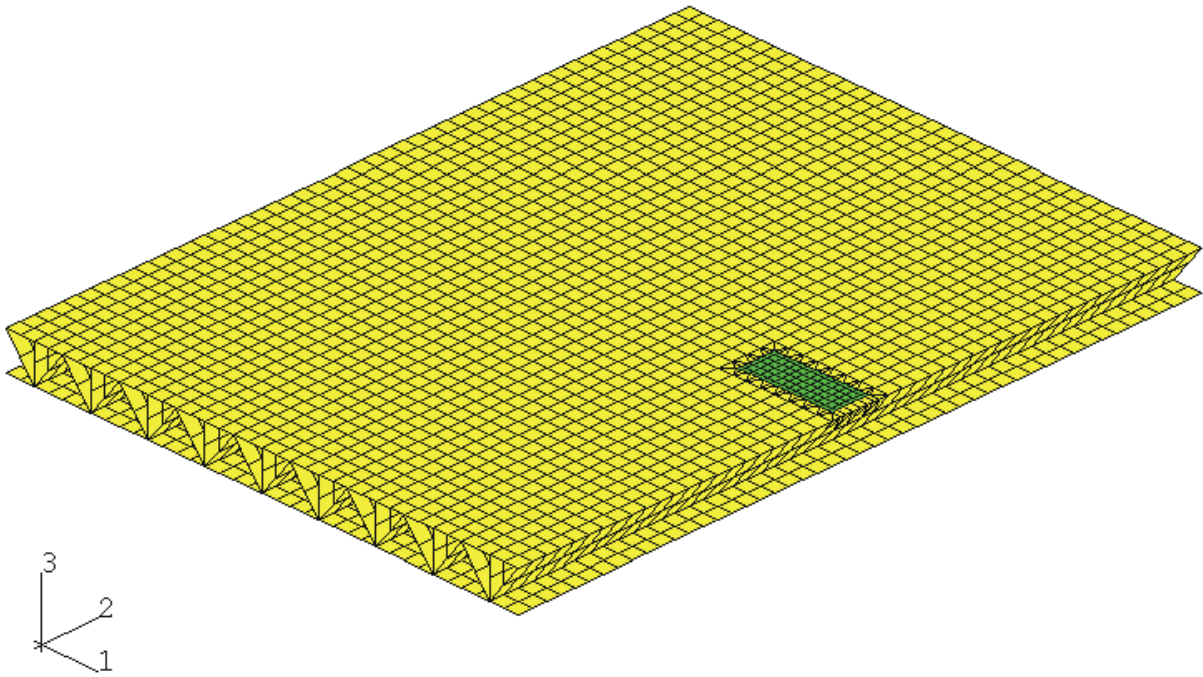


Figure 14. First Mesh For Load Case Four (3 X 3 Discretization With Two Rows of Elements Per Stiffener Height)

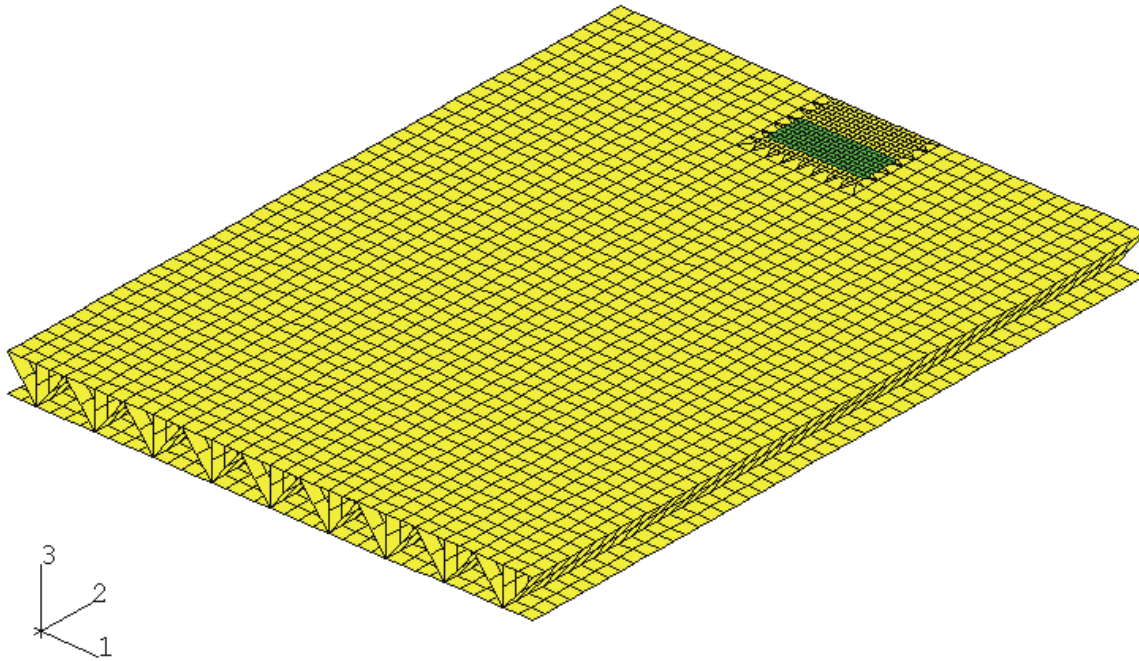


Figure 15. First Mesh For Load Case Five (3 X 3 Discretization With Two Rows of Elements Per Stiffener Height)

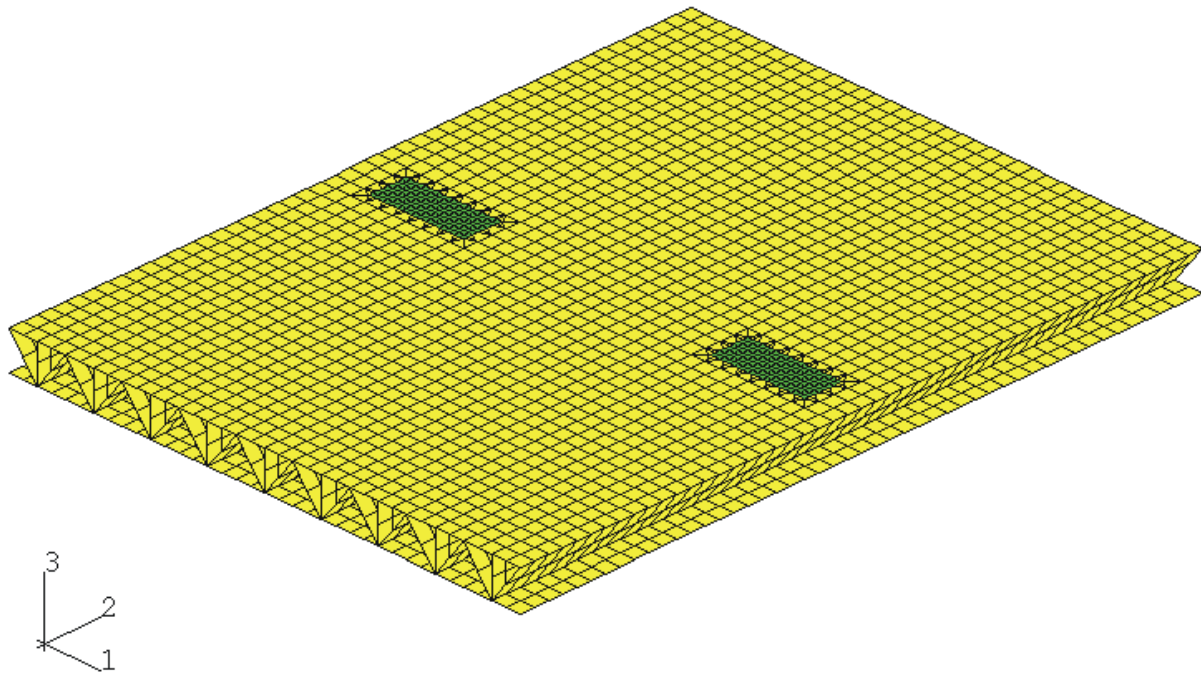


Figure 16. First Mesh For Load Case Six (3 X 3 Discretization With Two Rows of Elements Per Stiffener Height)

Shell elements, on the other hand, are specifically formulated to handle bending problems. As a result, many of the issues burdening continuum elements do not even arise in shell elements. ABAQUS contains many general-purpose shell elements suitable for a wide variety of analyses without requiring excessive specialization. HKS even recommends the use of shell elements to represent thin structural members (HKS, 1996). The combination of all of these issues lead to the use of shell elements to model the aluminum bridge deck panel.

Two specific shell elements were used in the panel models. First-order quadrilaterals employing reduced integration with hourglass control (ABAQUS element S4R) were used for the majority of the elements in the models. These four-noded elements allowed finite membrane strains and changes in shell thickness as the elements deformed. First-order triangles employing reduced integration (ABAQUS element S3R) were the other elements used in the panel models. These three-noded elements also allowed finite strains and changes in shell thickness as they deformed. These elements were used only to taper the mesh where necessary.

Both of these elements have six degrees of freedom per node and one integration point. Internal default algorithms were used to compute transverse shear stiffness and the hourglass control factor. Section behavior and thickness were defined by the *SHELL SECTION command. Using this command to specify section behavior forced ABAQUS to integrate through the thickness of the shell when evaluating the response. Integration through the thickness was performed using Simpson's rule.

Kinematics and Constitutive Theory

Data from the service-load tests showed that deck response was elastic and well within the linear region. Thus, rather simple kinematic and constitutive theories could be used in the models. Strains were computed with a linear kinematic relationship that was adequate for the small displacements and displacement gradients witnessed during these tests. Mechanical properties were defined as linear elastic. This linear elasticity was defined in ABAQUS by specifying the elastic modulus and Poisson's ratio. The nominal design values of 68.95 GPa (10,000,000 psi) and 0.3 were used.

Loading and Analysis

Elemental surface pressures were used to load the models because these surface pressures best simulated the manner in which the experimental loads were applied. The area of the load patch in the models was slightly smaller than the area of the load patch used in the laboratory evaluation. In the models, the load was applied over a rectangular region measuring 50.8 cm x 20.32 cm (20 in x 8 in). Although the area was slightly different, the magnitude of the force applied in the models was the same as that recorded in the laboratory.

The service load tests were simulated with a single-step analysis. Specifically, a static stress analysis was performed to obtain stress, strain, and displacement data. Since both the kinematic and constitutive theories used in the model were linear, the system of equations

generated by the model constituted a linear system. In ABAQUS, such a system was solved with a direct Gauss elimination method. A sparse solver was used to improve efficiency.

Model Validation

Models based upon the two meshes discussed were run for all seven load cases (a total of 14 simulations). Output used for validating the accuracy of the models was obtained first. Strain data were extracted from the models to compare with values measured by the rosettes attached to the panel. As an elemental output variable, strain values were acquired at the element integration points. To ensure an accurate comparison, output was acquired from the appropriate side of the element. Experimental values on the top deck surface were compared with data from the top section points, whereas strain values on the bottom deck surface were compared with data obtained at the bottom section points.

Despite these efforts to promote accuracy, the layout of the mesh prevented direct comparison. The element integration points rarely coincided with the exact location of the strain rosettes. To circumvent this situation, strain data were obtained for elements surrounding the rosette and averaged to yield values at the desired location. This averaging process was performed outside of the ABAQUS program using a linear interpolation scheme. Strain data from 38 rosettes were used to calibrate the models. The 38 rosettes used for calibration were those lying along the panel centerlines. Rosettes lying on the longitudinal centerline that were parallel to the extrusions (and parallel to the 3.66 m sides) were referred to as gages in the longitudinal strip. Rosettes attached to the centerline perpendicular to the extrusions (and perpendicular to the 3.66 m sides) were referred to as gages in the transverse strip. These strips are illustrated in Figure 17. Their distance from the geometric center of the panel identifies specific gages within these strips.

Rosettes within these strips measured strain in both the longitudinal and transverse directions. The value being discussed was referred to as either longitudinal strain or transverse strain. As an example, one may consider Figure 18. The rosettes lay along a transverse strip. If strain in the direction of the arrow on the bottom deck surface was being discussed, the data were identified as bottom of panel, longitudinal strain across transverse strip. Eight data sets like this were used to calibrate the models. The eight sets arise from a transverse strip and a longitudinal strip on both the top and bottom deck surfaces. Within these strips, strains were measured in two directions. Thus, four strips with two variables per strip resulted in eight sets of data.

Deflection data were also used to assess model accuracy. Unlike the rosettes, the deflection gages were not permanently attached to the deck. This allowed the gages to be repositioned at essential locations for each load test. As a result, the nodes used to obtain deflection data varied with each load case. As with the strain gages, the location of the deflection gages rarely coincided with nodal positions. To overcome this problem, displacements were obtained at nodes surrounding the specific location and then interpolated to the exact position.

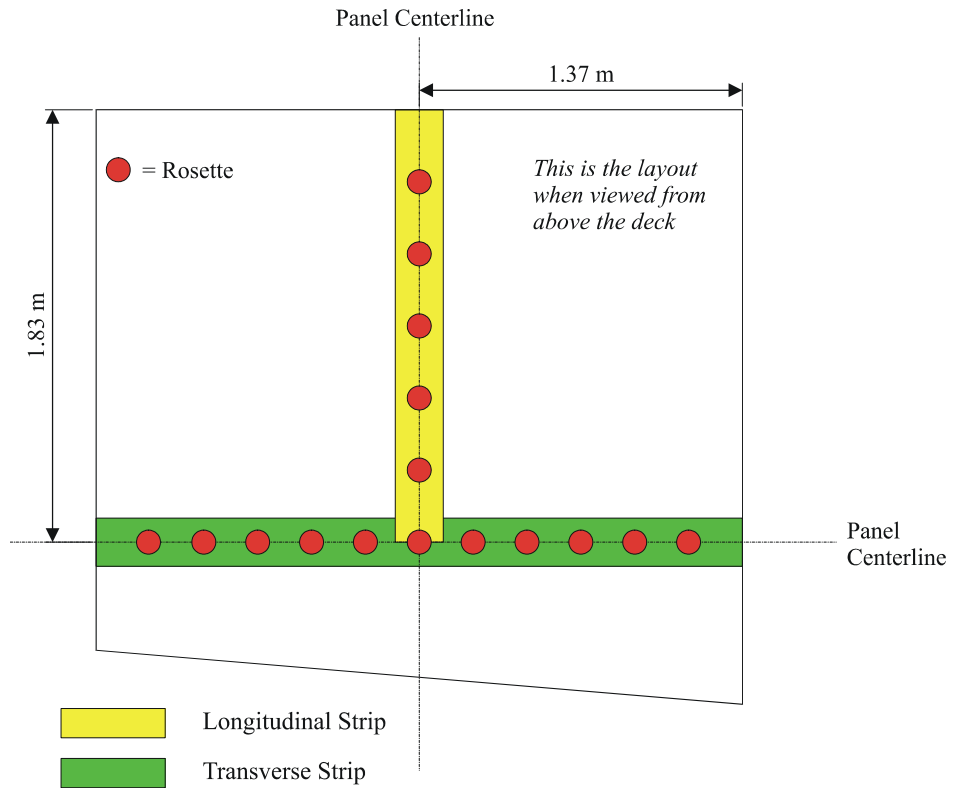


Figure 17. Nomenclature of Calibration Strips

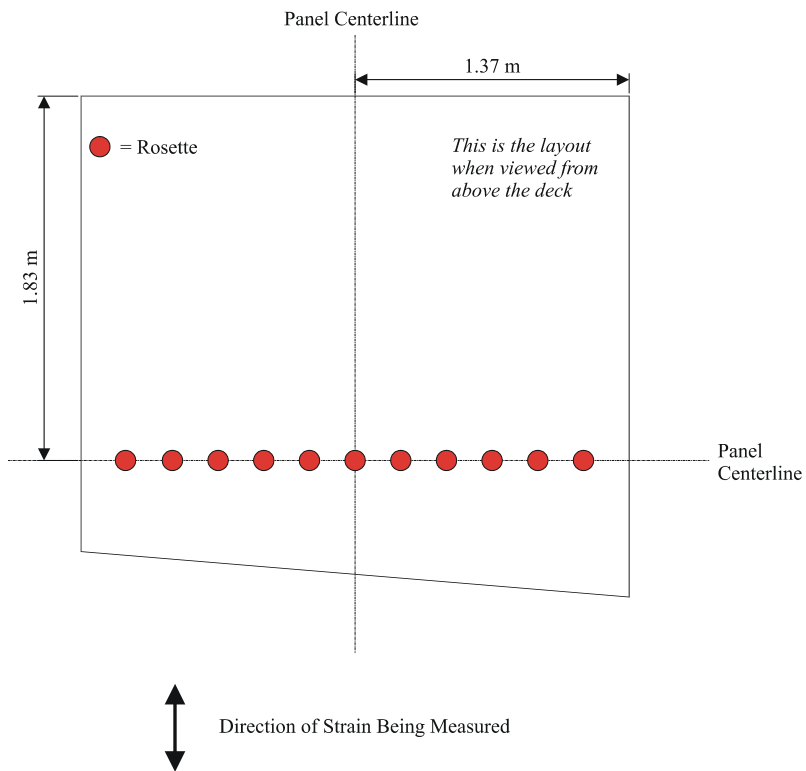


Figure 18. Example of Calibration Nomenclature

RESULTS AND DISCUSSION

As noted earlier, each of the seven load cases was modeled using two different finite element meshes. Each of these 14 models was then validated by comparing predicted and measured strain and displacement data using the procedures described in the previous section. Although this validation process is important, only the results from one load case are presented in this report. The results from load case 7 are presented in Figures 19 through 22 and Table 1. Discussing load case 7 is beneficial because the support conditions were the same as those present in an actual bridge. Also, the configuration of load case 7 was similar to that of the ultimate load tests described in the upcoming report on Phase 2 of this project. In the figures, 3×3 refers to the model using 7.62 cm (3 in) elements on the deck surfaces, and 2×2 refers to the models using 5.08 cm (2 in) elements on the deck surfaces. As observed from the graphs, the model behavior agreed well with both the magnitudes and the distributions of the strains measured during the laboratory tests.

Examination of the deflection data given in Table 1 indicates that the displacement predictions were consistently less than the measured deflections for load case 7. Although the differences appear small, the percentage error in these deflections was roughly 25%. This high error was attributable to the rigid body motion of the panel. In this simply supported load case, the panel did not rest flush on the supports and was observed to displace substantially under even low loads. By subtracting out this apparent rigid body motion from the experimental data, the measured and predicted displacement data were then found to compare favorably.

Once it was determined that the models could predict actual panel behavior with reasonable accuracy, efforts were focused on employing the calibrated models to analyze panel stresses. The researchers were interested in both the magnitudes and distributions of stress developed under the various service load conditions. To analyze these variables efficiently, the graphical post processor (ABAQUS/POST) was used to generate contour plots of the stresses generated in the deck.

Two steps were taken to ensure that accurate contour plots were generated. To identify the extreme values in specific components of the deck, individual element sets were analyzed one at a time. Four specific element sets were monitored in each simulation: the top deck surface, the bottom deck surface, the vertical stiffeners, and the inclined stiffeners. The element sets were analyzed individually. Additionally, stress values at the element integration points were plotted without averaging values across elemental boundaries. Although this created jagged contours, the resulting plots were more indicative of the stresses present in the elements.

Table 2 summarizes the maximum stresses developed in each element set, and Table 3 lists the allowable stresses for the design that were computed by Modjeski and Masters (1996). For the top and bottom deck surfaces, longitudinal stress and transverse stress obeyed the direction nomenclature illustrated in Figure 11. Unfortunately, the orientation of the stiffeners resulted in output that did not completely coincide with this system. Stress data still could have been obtained in the longitudinal direction, but the other stress variable subsequently measured stress in the vertical or inclined direction of the stiffeners. This new direction of stress was referred to as the vertical stress and is illustrated in Figure 23.

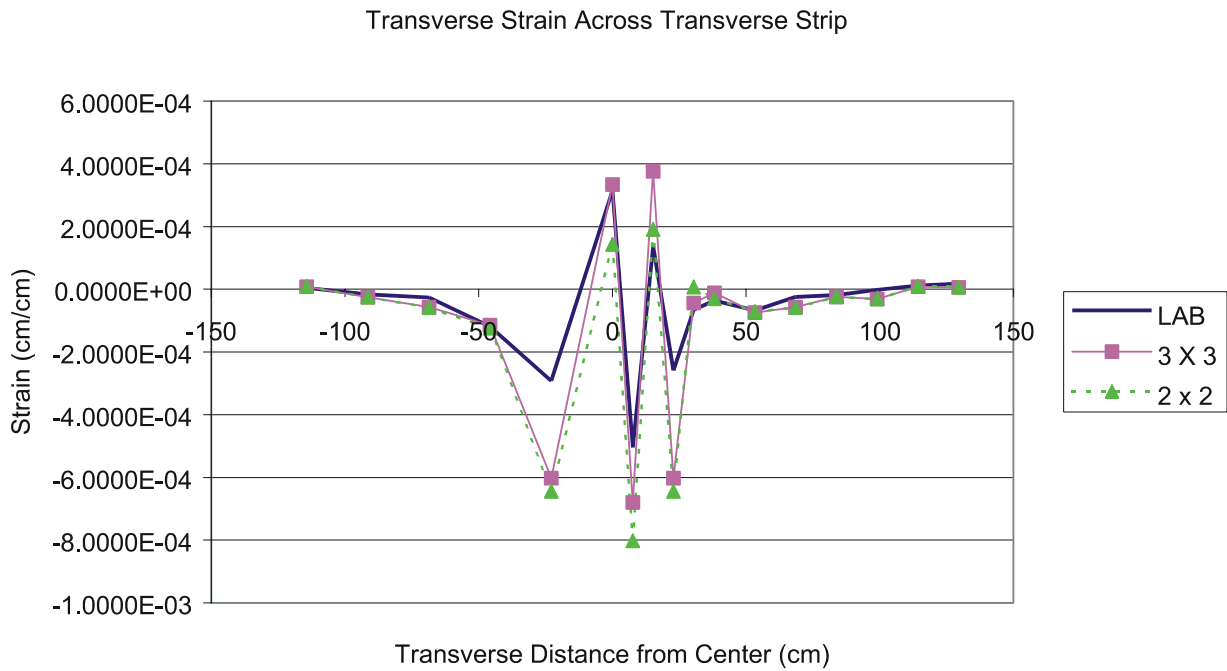
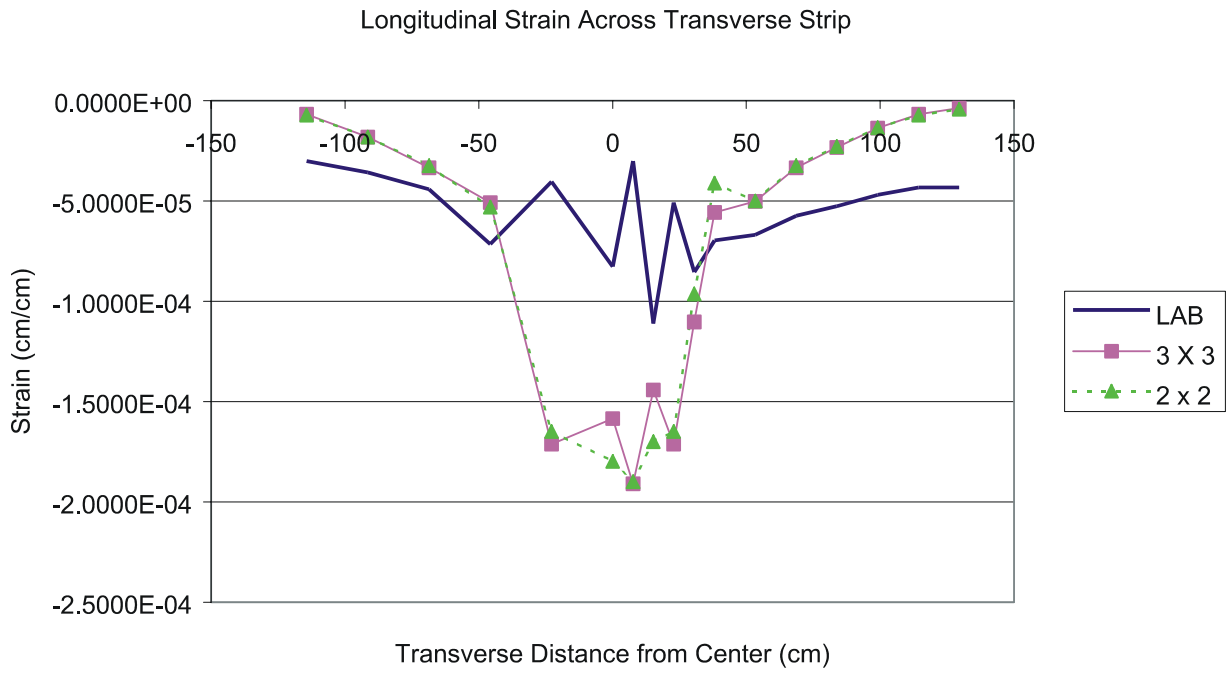


Figure 19. Model Verification—Load Case Seven, Top Deck Surface, Transverse Strip

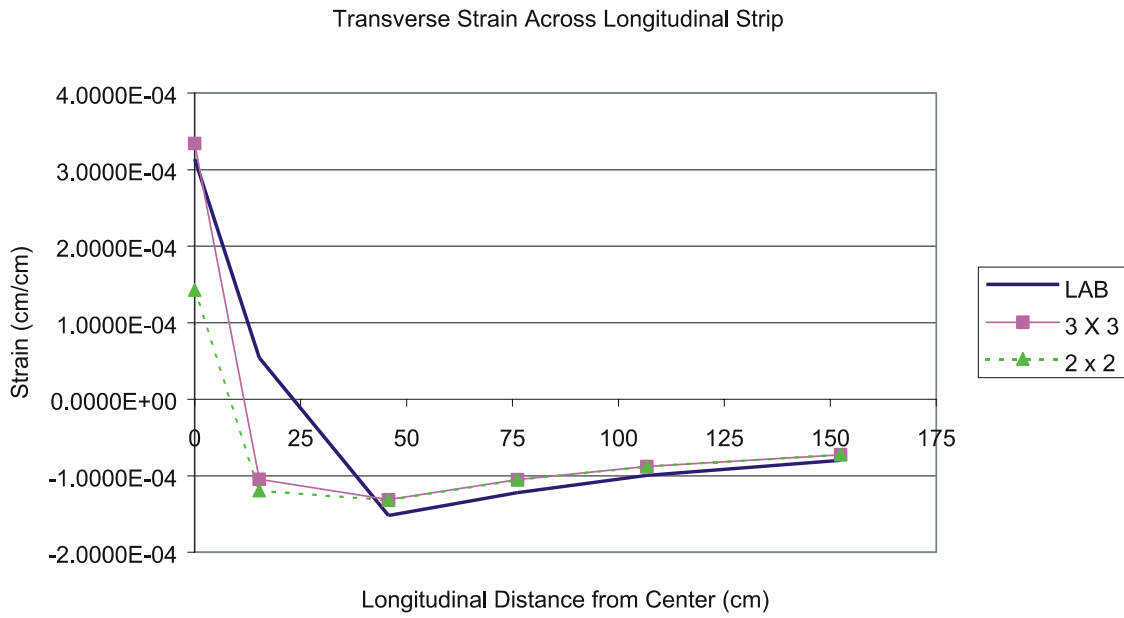
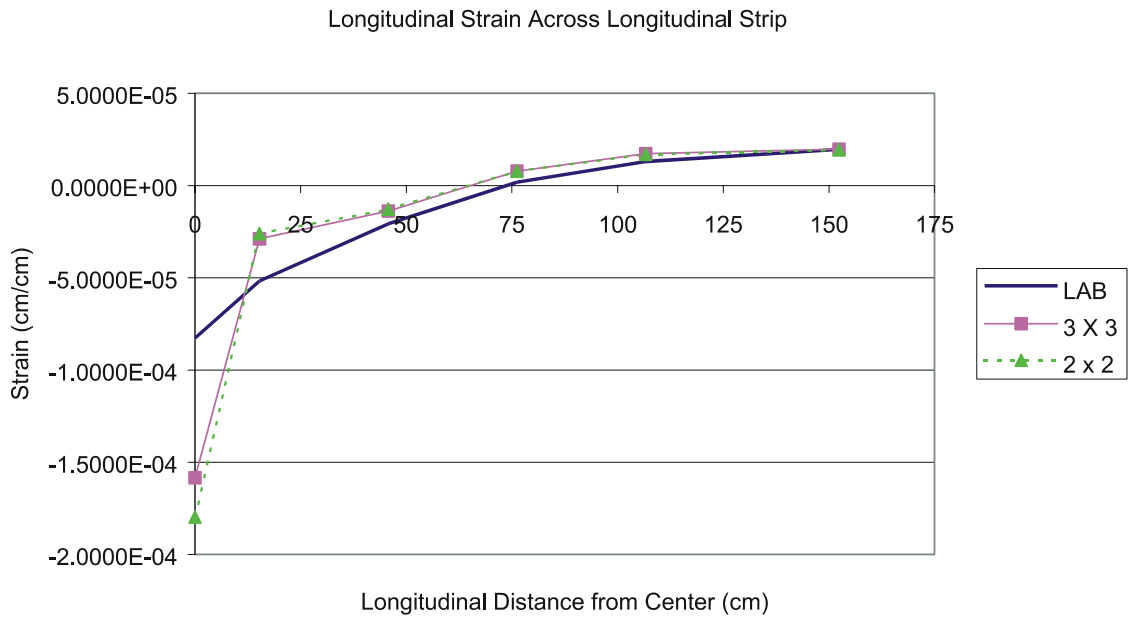


Figure 20. Model Verification—Load Case Seven, Top Deck Surface, Longitudinal Strip

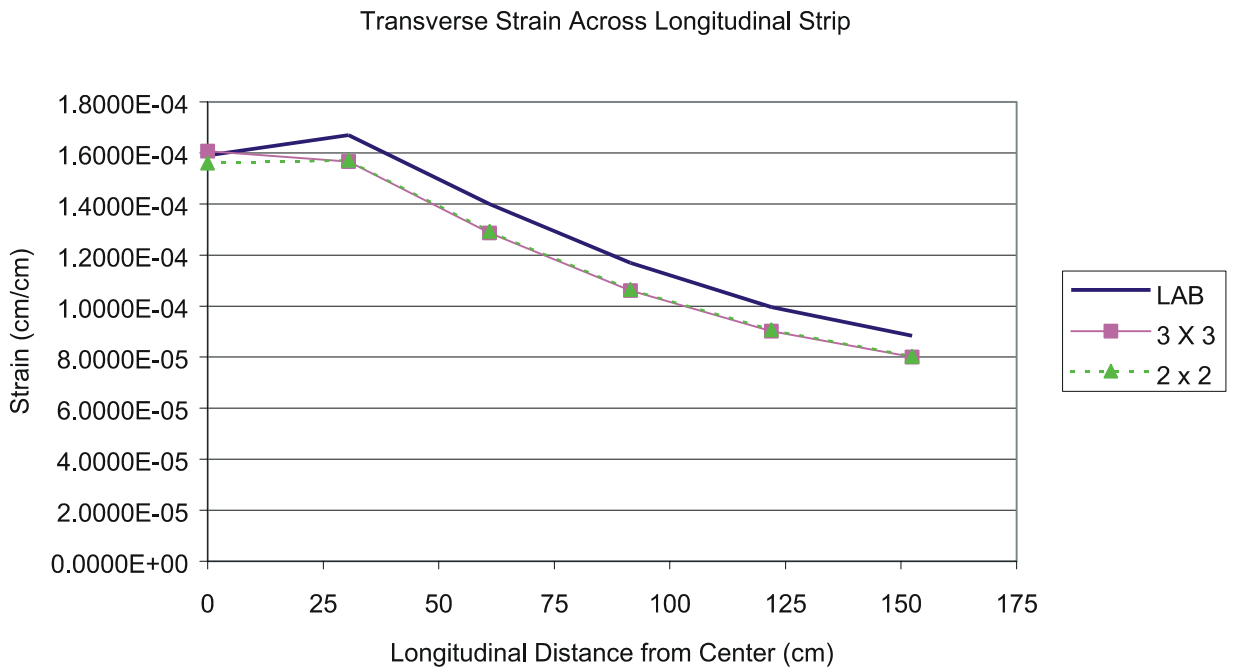
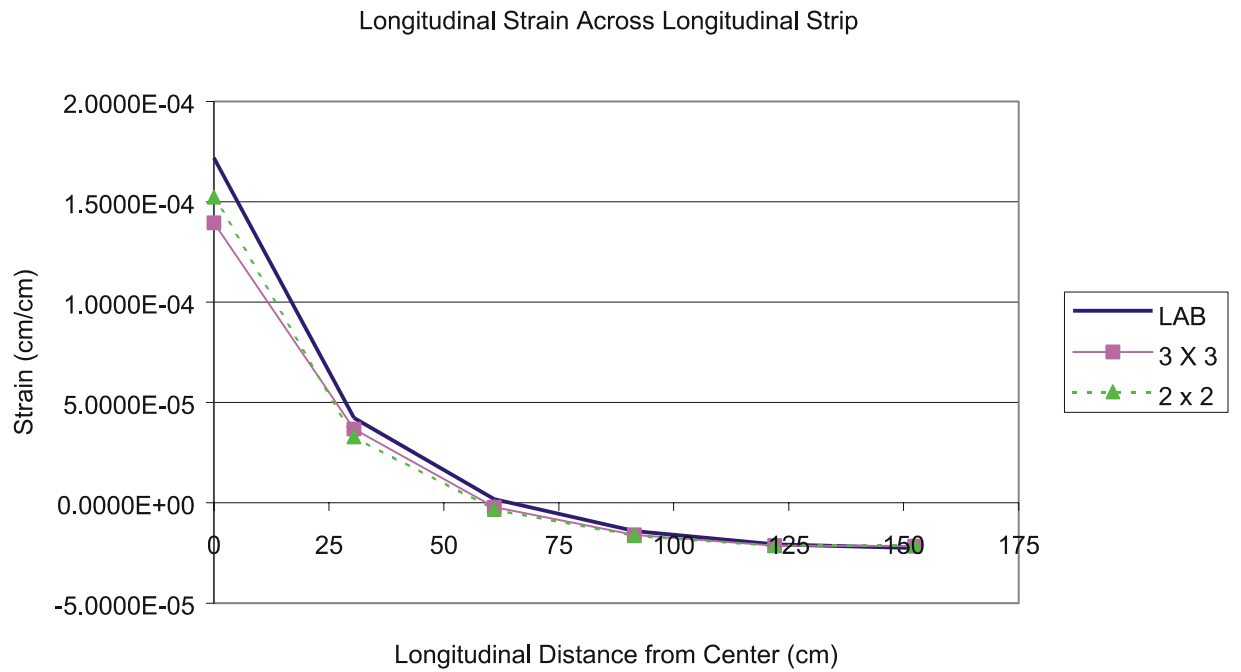


Figure 21. Model Verification—Load Case Seven, Bottom Deck Surface, Transverse Strip

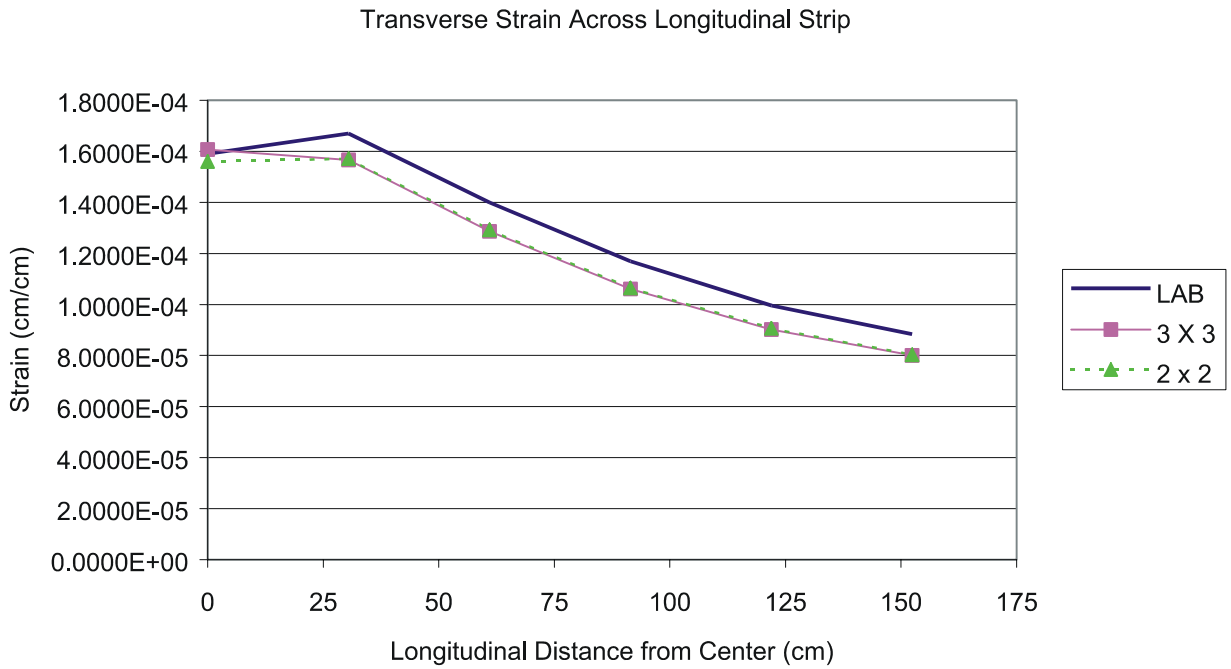
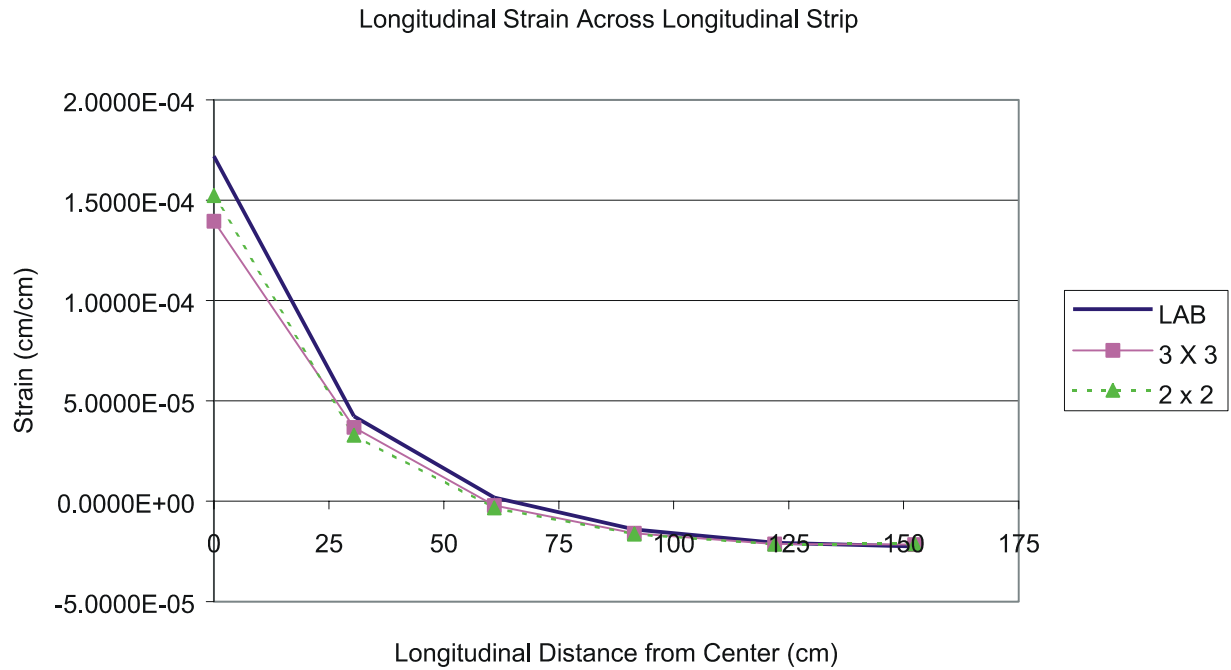


Figure 22. Model Verification—Load Case Seven, Bottom Deck Surface, Longitudinal Strip

Table 1. Model Verification —Load Case 7 (Displacements)

Gage Number	LAB Displacements (cm)	FEM Displacements (cm)	
		3 x 3 Model	2 x 2 Model
1	-0.156	-0.099	-0.099
2	-0.134	-0.064	-0.064
3	-- ^a	-0.053	-0.053
4	-0.119	-0.064	-0.064
5	-0.132	-0.053	-0.053
6	-0.070	-0.045	-0.045
7	-0.089	-0.045	-0.045

^aGage 3 was damaged and produced erroneous data.

Table 2. Maximum Stresses Developed During Load Case 7

Deck Component	Type of Stress	Maximum Stresses (MPa)		
		3 x 3 Model	2 x 2 Model	Location
Top Deck Surface				
Transverse Stress	Compression	56.02	65.11	Under load patch
	Tension	27.79	13.73	Under load patch
Longitudinal Stress	Compression	30.19	32.62	Under load patch
	Tension	0.16	0.17	Toward panel edges
Bottom Deck Surface				
Transverse Stress	Compression	-0.59 ^a	0.21	Edges over SS
	Tension	15.60	15.59	Center of panel
Longitudinal Stress	Compression	-0.03 ^a	0.30	Toward panel edges
	Tension	14.23	15.09	Under load patch
Vertical Stiffeners				
Vertical Stress	Compression	22.25	27.08	Under load patch
	Tension	4.17	5.88	Various locations
Longitudinal Stress	Compression	13.84	10.89	Under load patch
	Tension	4.33	6.81	Under load patch
Inclined Stiffeners				
Vertical Stress	Compression	21.68	24.73	Under load patch
	Tension	11.75	12.20	Under load patch
Longitudinal Stress	Compression	13.91	11.33	Under load patch
	Tension	7.48	10.11	Under load patch

^aNo compressive stresses were generated; these are the smallest tensile stresses.

Table 3. Design Allowable Stresses

Deck Component	Allowable Stress (MPa)			
	System I Stresses	System II Stresses		System III Stresses
		Tensile	Compressive	
Top Deck Surface	93.08	40.68	80.67	121.35
Bottom Deck Surface	82.05	40.68	30.34	-- ^a
Vertical Stiffeners	121.35	93.08	50.33	-- ^a
Inclined Stiffeners	121.35	40.68	20.68	-- ^a

^aSystem III stresses are local stresses that occur only in the top deck chord.

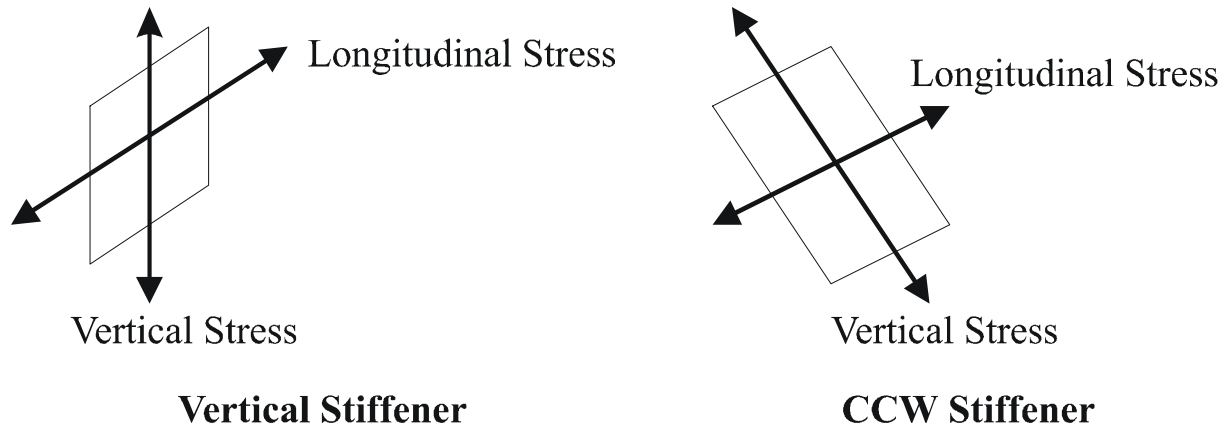


Figure 23. Stress Nomenclature in the Stiffeners

As the data in the tables show, models based upon the two meshes yielded similar results. Both models predicted similar stress distributions, and away from the load patch, similar maximum values occurred. Closer examination of the stresses on the bottom deck surface demonstrated that the models produced nearly identical results. This was expected because the bottom deck surface was essentially unaffected by localized forces.

Two types of stresses are of interest for each load case: the maximum stresses developed in the panel, and those stresses closest to the design allowables. The largest stresses predicted by the two models are summarized in Tables 4 and 5. For the model based upon the 3 x 3 mesh, the maximum stresses (both tensile and compressive) occurred on the top deck surface under the load patch. All of these stresses were System III stresses, induced by localized bending of the top deck flange. Models using the 2 x 2 mesh predicted slightly different maximum values. The largest compressive stresses were still produced on the top deck surface by localized bending under the load patch. Magnitudes of these compressive stresses were similar to those predicted by the model based upon the 3 x 3 mesh. For load case 7, the largest tensile stresses also occurred on the bottom deck surface and were a result of localized bending.

Table 4. Largest Stresses Predicted by the 3 x 3 Model

Load Case	Description of Stress		
	Stress (MPa)	Location	Characterization
Compressive			
7	56.02	Top Deck Surface, Under Load Patch	System III
Tensile			
7	27.79	Top Deck Surface, Under Load Patch	System III

Table 5. Largest Stresses Predicted By The 2 X 2 Model

Load Case	Description of Stress		
	Stress (MPa)	Location	Characterization
Compressive			
7	65.11	Top Deck Surface, Under Load Patch	System III
Tensile			
7	15.59	Bottom Deck Surface, Center of Panel	System II

Although the models predicted slightly different maximum stresses for the various load cases, both models show the significance of the localized deformation. To understand the significance of these local stresses, one must first consider the global bending stresses developed on the bottom deck surface for load case 7. For the model using a 3 x 3 mesh, the maximum tensile stresses on the bottom deck surface were on the order of 15 MPa (2400 psi). On the top deck surface, localized deformation generated maximum tensile stresses were on the order of 28 MPa (4900 psi). This meant that the local bending stresses were approximately 2 times larger than the global bending stresses. Matteo et al. (1997) derived a ratio of 1.6 from experimental strain values.

Although the models based upon the 2 x 2 mesh predicted different maximum stresses, close examination of the data showed that localized bending stresses were still significant. The average ratio of local tensile stress to global tensile stress was approximately 0.9. Although the global stresses were larger, this ratio was rather high and underscored the importance of the localized effects.

Despite these high localized stresses, the magnitudes were still well within the allowable stresses for the designs that are listed in Table 3. However, the vertical compressive stresses in the stiffeners were much closer to the allowable values for the design (Table 6). Because of the geometric arrangement of this structure, the stiffeners acted like thin plates subject to lateral loading. As with any thin member subject to compressive loading, stability was a legitimate concern. This fact was evident when the design allowable stress was examined; the permissible compressive stresses in the stiffeners were rather low because of the high buckling potential.

Table 6. Average Maximum Vertical Compressive Stresses Developed in the Stiffeners

Stiffeners	Average Stresses (MPa)	
	3 x 3 Model	2 x 2 Model
Vertical	23.65	28.68
Inclined	23.58	25.04

CONCLUSIONS

- The findings in this study showed that properly developed models could reliably predict the complex response of the aluminum bridge deck panel. Both strain distributions and magnitudes were predicted with reasonable accuracy. On the bottom deck surface, the average difference between strain values predicted by the models and those measured in the laboratory was 22 microstrain for load cases involving simple supports and 55 microstrain for load cases involving cantilevered supports. Excluding output obtained under the load patch, the average difference in strains on the top deck surface was 24 microstrain for simply supported load cases and 59 microstrain for load cases involving cantilevered supports
- The authors suspect that the stresses developed in the inclined stiffeners did not reach unacceptable levels. Several factors supported this conclusion. The large stress values predicted by the model all occurred in the upper portion of the stiffeners. As the verification process showed, strains on the top deck surface were predicted on the average within 53 microstrain for the simply supported load cases and within 75 microstrain for the cantilevered load cases. These strain discrepancies corresponded to stress differences of 3.65 MPa (530 psi) and 5.17 MPa (750 psi), respectively. If these stress differences are subtracted from the model predictions, the stresses are determined to be below the design limits. The authors believe the stress errors should be subtracted because the stiffeners in question are under the load patch. In the vicinity of the load, the model tended to predict much larger stress and strain quantities than those recorded during the laboratory tests. Not only did the analytical model predict higher values in the vicinity of the load, but also the discrepancies themselves became larger. Thus, the average corrections applied, as mentioned previously, may be conservative.
- Models based upon both meshes predicted that the largest compressive stresses would occur under the load patch for all load cases. These stresses resulted from localized bending of the top deck flange (System III stresses).
- The largest tensile stresses predicted by models with a 3 x 3 mesh were also obtained on the top deck surface under the load patch. Again, localized bending of the top deck chord generated these large values.
- The location of the largest tensile stresses predicted by models with a 2 x 2 mesh varied among the load cases. Maximum tensile stresses corresponding to each stress system were witnessed for different load cases.
- Vertical compressive stresses developed in the inclined stiffeners were rather high compared to design allowables.
- Except for the uncertainty regarding the stresses in the inclined stiffeners, the panel satisfied all design criteria. Stresses generated in the remaining members were well below the allowable values, and deflections did not exceed serviceability requirements.

- Results from the model were in excellent agreement with the model developed by Reynolds. Although proprietary constraints prevented a specific comparison, stress distributions and magnitudes were very similar. The deflections predicted by both models were almost identical.
- Economic considerations were not addressed in this study.

RECOMMENDATIONS

1. The recommendation was made to the VDOT Structure and Bridge Division to construct the replacement structure carrying Route 58 over the Little Buffalo Creek in Mecklenburg County. This was the first field application of the aluminum deck system.
2. VDOT and FHWA should consider this system of aluminum decks as an alternative to conventional cast-in-place reinforced concrete deck systems from a structural behavior perspective.

REFERENCES

- Cook, R.D., Malkus, D.S., & Plesha, M.E. (1989). *Concepts And Applications of Finite Element Analysis* (3rd ed.). New York: John Wiley and Sons.
- Hibbitt, Karlsson, & Sorensen, Inc. (1996). *ABAQUS/Standard Update Manual: Example Problems, Verification, Theory; Version 5.6*. Rhode Island: Hibbitt, Karlsson, and Sorensen, Inc.
- Kissell, J.R. & Ferry, R.L. (1995). *Aluminum Structures—A Guide To Their Specifications And Design*. New York: John Wiley and Sons.
- Matteo, A.D., Massarelli, P.J., Gomez, J.P., Wright, W., & Cooper, J. (1997). Preliminary Evaluation Of An Aluminum Bridge Deck Design For Highway Bridges. In *Seventh Conference on Structural Faults and Repair*. Edinburgh, Scotland.
- Modjeski & Masters, Inc. (1996). *Index of Calculations for VDOT Bridge Rehabilitation—Rt. 58 Over Little Buffalo Creek*. Unpublished calculations from Modjeski and Masters, Inc. Harrisburg, PA.
- New Aluminum Decks Cut Loads, Add Life. (1996). *ASCE Civil Engineering*, 66, No. 8, p. 12.

- O'Connor, D.S. (1995). Review Of The Life Cycle Cost Issues Relating to Prefabricated Aluminum Bridge Decks. Paper for Reynolds Metals Company. May 27, 1995.
- Segerlind, L.J. (1976). *Applied Finite Element Analysis*. New York: John Wiley & Sons.
- Sharp, M.L. (1993). *Behavior and Design of Aluminum Structures*. New York: McGraw-Hill.
- Sotiropoulos, S.N. & GangaRao, H.V.S. (1993). *Design Anomalies In Concrete Deck-Steel Stringer Bridges*. (Report No. TRR 1393). Washington, D.C.: Transportation Research Board.
- The Aluminum Association. (1996). *Aluminum Alloys for Bridges: Extending the Life of U.S. Bridges*. Washington, DC: Author.
- Wolchuk, R. (1987). Applications Of Orthotropic Decks In Bridge Rehabilitation. *Engineering Journal*, 24, No. 3, pp. 113-121.